



Modeling the influence of carbon branching structure on SOA formation via multiphase reactions of alkanes

Azad Madhu¹, Myoseon Jang¹, Yujin Jo¹

¹Engineering School of Sustainable Infrastructure and Environment, University of Florida, Gainesville, 32608, United States of America

Correspondence to: Myoseon Jang (mjang@ufl.edu)

Abstract.

Branched alkanes represent a significant proportion of hydrocarbons emitted in urban environments. To accurately predict the SOA budgets in urban environments, these branched alkanes should be considered as SOA precursors. However, the potential to form SOA from diverse branched alkanes under varying environmental conditions is currently not well understood. In this study, the Unified Partitioning Aerosol Phase Reaction (UNIPAR) model is extended to predict SOA formation via the multiphase reactions of various branched alkanes. Simulations with the UNIPAR model, which processes multiphase partitioning and aerosol phase reactions to form SOA, require a product distribution predicted from an explicit gas kinetic mechanism, whose oxygenated products are applied to create volatility-reactivity based lumping species array. Due to a lack of practically applicable explicit gas mechanisms, the prediction of the product distributions of various branched alkanes was approached with an innovative method that considers carbon lengths and branching structures. The lumping array of each branched alkane was primarily constructed using an existing lumping array of the linear alkane with the nearest vapor pressure. Generally, the vapor pressures of branched alkanes and their oxidation products are lower than those of linear alkanes with the same carbon length. In addition, increasing the branching of an alkane can also decrease the ability of alkanes to undergo autoxidation reactions that tend to form low-volatility products and significantly contribute to alkane SOA formation. To account for this, an autoxidation reduction factor, as a function of the degree and position of branching, was applied to the lumped groups which contain autoxidation products. The resulting product distributions were then applied to the UNIPAR model for predicting branched alkane SOA formation. The simulated SOA mass was compared to SOA data generated under varying experimental conditions (i.e., NO_x levels, seed conditions, and humidity) in an outdoor photochemical smog chamber. Branched alkane SOA yields were significantly impacted by NO_x levels but insignificantly impacted by seed conditions or humidity. The SOA formation from branched and linear alkanes in diesel fuel was simulated to understand the relative importance of branched and linear alkanes in a wide range of carbon numbers. Overall, branched alkanes account for more SOA mass than linear alkanes due to their higher contribution to diesel fuel. As anthropogenic emissions of hydrocarbons decrease, biogenic precursors tend to become increasingly important with regard to atmospheric organic aerosol. Unlike aromatics, which are almost exclusively sourced from anthropogenic emissions, alkanes can also be emitted from biogenic sources (i.e. plant wax) and they will remain a significant source of SOA.



1 Introduction

35 Secondary Organic Aerosol (SOA) in the atmosphere, formed via the atmospheric oxidation of various precursor hydrocarbons (HCs), serves a considerable role in climate, cloud formation, and human health (Nel, 2005; Shrivastava et al., 2017; World Health, 2016; Epa, 2019). Precursor HCs found in ambient air are emitted through a variety of both anthropogenic and biogenic sources. Alkanes are one of the major classes of precursor HCs typically found in urban environments, emitted from anthropogenic sources such as fossil fuels, personal care products, paints, and pesticides (Li et al., 2022; Wu et al., 2019). In addition to anthropogenic sources, plant wax has also been identified to be a significant source of atmospheric alkanes (Alves et al., 2012). Several recent gas sampling studies have identified alkanes as one of the two dominant sets of HCs measured in urban environments, alongside aromatics (Massolo et al., 2010; Song et al., 2019; Xuan et al., 2021; Zhao et al., 2020). This is consistent with Caplain et al.'s (2006) study which reported that alkanes represent significant proportions of both gasoline and diesel fuel exhaust. Additionally, recent regional modeling studies have shown 45 that alkanes are also one of the dominant sources of secondary organic aerosol (SOA) formation in urban environments (Li et al., 2022; Jo et al., 2023; Yang et al., 2019). Within the set of alkanes, branched alkanes represent larger proportions of both gasoline and diesel fuels compared to linear alkanes (Caplain et al., 2006). Furthermore, intermediate-volatility organic compounds (IVOCs) in the atmosphere are largely composed of an unresolved complex mixture, which is likely to consist of a variety of branched alkane isomers (Tkacik et al., 2012).

50 Currently available mechanisms of branched alkanes are either overly simplistic, with a limited set of oxidation products (Lim and Ziemann, 2009), or overly complex, with too many products to be incorporated into an SOA model (i.e. GECKOa). Some studies have managed to model the SOA formation of various branched alkanes using the GECKOa model (Aumont et al., 2013; La et al., 2016). However, because the number of oxidation products in the GECKOa model increases exponentially as the number of carbons of the HC precursor increases, these studies had significant limitations as they tried 55 to reduce the number of products to a manageable value. For example, La et al. (2016) reduced the number of products considered in the model by limiting the experimental time to a maximum of 1 hour. Aumont et al. (2013) reduced the number of precursors considered by only considering the High NO_x condition, a limitation which they acknowledge is a “severe simplification.” For application to a regional model, parameters generated from chamber models must be applicable for a variety of NO_x conditions for the whole range of oxidation products generated throughout a long oxidation time.

60 In recent chamber study by Madhu et al. (2023), the SOA formation of a series of linear alkanes was simulated for a wide range of carbon numbers using the UNified Partitioning Aerosol Reaction (UNIPAR) model, which simulates SOA mass via multiphase reactions of HCs. The UNIPAR model utilizes lumping arrays generated from explicitly predicted gas oxidation products. The volatility-reactivity based lumping species in the model are applied to multiphase partitioning and aerosol phase reactions to form SOA mass (Choi and Jang, 2022; Han and Jang, 2022; Im et al., 2014; Yu et al., 2021; Zhou et al., 65 2019). In order to predict SOA mass originating from linear alkanes at different carbon lengths, an incremental volatility coefficient (IVC) was used to predict the lumping arrays of larger linear alkanes without explicit mechanisms (Madhu et al.,



2023). In their model simulation, the importance of low-volatility autoxidation products in linear alkane SOA formation was demonstrated.

70 The molecular structure of an alkane serves an important role in its capability to form SOA mass. Linear and branched alkanes tend to have similar oxidation products, with the distinction that branched alkane products tend to be more volatile at the same precursor carbon number (Lim and Ziemann, 2009). Additionally, the presence of some alkyl branches can decrease the ability of alkanes to participate in autoxidation reactions and increase the decomposition of intermediate products, which further reduces SOA yields by decreasing the amount of low-volatility oxidation products formed.

In this study, the UNIPAR model is used to simulate the SOA formation from the multiphase reactions of branched alkanes.
75 Due to a lack of practically applicable explicit gas mechanisms, the product distributions of branched alkanes were constructed primarily using the product distributions of linear alkanes with the nearest vapor pressure. To account for the reduction of probability for autoxidation reactions, an autoxidation reduction factor, which is a function of the degree of branching and position, was applied to the construction of lumping groups that include autoxidation products. Predicted lumping arrays for various branched alkanes (Isododecane, Trimethyldodecane, Heptamethylnonane, and
80 Tetramethylpentadecane) were used to simulate SOA formation, which was compared to chamber generated SOA data. The sensitivity of branched alkane SOA yields to humidity, NO_x conditions, seed conditions, and branching structure at given simulation conditions was projected. Additionally, a simulation of SOA formation from branched and linear alkanes found in diesel was used to determine their relative significance as SOA precursors.

2 Experimental section

85 Alkane SOA was produced from photooxidation of a set of branched alkanes [Isododecane (Sigma-Aldrich; 80%), Trimethyldodecane(Sigma-Aldrich; 99%), Heptamethylnonane(Sigma-Aldrich; 98%), Tetramethylpentadecane(Fisher Scientific; 95%)] using the UF-APHOR dual chamber (52 m³ each) located at the University of Florida. The detailed description of the operation of the large outdoor smog chamber can be found in a previous study (Im et al., 2014). Table 1 summarizes the experimental conditions of outdoor chamber experiments. Precursor alkane hydrocarbons (HCs) were
90 injected into chamber through evaporation via heating. CCl₄ (Sigma-Aldrich; ≥99.5%), was introduced into the chamber as a non-reactive gas which is used to measure chamber dilution. HONO was used as a source of hydroxyl radicals in the chamber. HCs, HONO, and NO (2% in N₂, Airgas Inc., USA) and inorganic seed were introduced into the smog chamber before sunrise. Experiments were performed under two different NO_x levels (high NO_x: HC/NO_x <5 ppbC/ppb; low NO_x: HC/NO_x >10 ppbC/ppb) and three different seed conditions (without seed, sulfuric acid, and ammonium sulfate).
95 Concentrations of gas phase HCs and CCl₄ were measured using a GC-FID (7820A, Agilent Technologies, Inc., USA). Concentrations of ozone and NO_x within the chamber were measured using a photometric ozone analyzer (400E, Teledyne Technologies, Inc., USA) and a chemiluminescence NO/NO_x analyzer (T201, Teledyne Technologies, Inc., USA), respectively. Experiments using inorganic seed employed a Particle into liquid sampler (ADISO 2081, Applikon Inc., USA)



integrated with Ion Chromatography (Compact IC 761, Metrohm Inc., Switzerland) (PILS-IC) to measure inorganic ion
100 concentrations within the chamber. The size distribution of particles within the chamber was measured using a scanning
mobility particle sizer (SMPS 3080, TSI Inc., USA).

Previous studies that have measured the density of alkane SOA have found a range from 1 to 1.4 g/cm³ (Li et al., 2020; Li et
al., 2022; Lim and Ziemann, 2009; Loza et al., 2014). Aerosols from each alkane experiment in this study were assumed to
have a density of 1.2 g/cm³. A hygrometer (CR1000 measurement and control system, Campbell Scientific Inc., USA) was
105 used to measure meteorological factors (temperature, relative humidity (RH) and an ultraviolet radiometer (TUVB, Eppley
Laboratory Inc., USA) was used to measure sunlight intensity. An organic carbon/elemental carbon analyzer (OC/EC model
4, Sunset Laboratory Inc., USA) was used to measure the concentration of organic carbon in aerosol every 50 minutes. The
concentration of organic matter in aerosol (OM, $\mu\text{g m}^{-3}$) was then calculated based on the OC concentration predicted by the
UNIPAR model and an OM to OC ratio. The OM to OC ratio of SOA from alkane species decreased as the chain length
110 increased. The concentrations of OM measured from the chamber were corrected for chamber dilution using a dilution factor
and for particle wall loss to the chamber wall using a particle loss factor. An aerosol chemical speciation monitor (ACSM,
Aerodyne Research Inc., USA) was used to measure the aerosol composition (sulfate, nitrate, ammonium, and OM). The
compositions obtained from the ACSM were compared with measurements from the OC/EC and the PILS-IC. SOA yields
(*Y*) were then calculated as the final measured concentration of OM divided by the total consumption of HC precursors. In
115 order to characterize the chemical functional distribution of SOA, chamber-generated SOA was collected on a silicon disk
(13 × 2 mm, Sigma-Aldrich, USA) using a home-built impactor and analyzed using the FTIR spectrometer (Nicolet iS50,
Thermo Fisher Inc., USA) in transmission mode. The FTIR disc was weighed using an analytical balance before and after
particle impaction to measure particle mass collected.



120

Table 1. Summary of experimental conditions and observed data for experiments performed in the UF-APHOR outdoor chamber.

Label	Date	HC name	Initial NO _x (PPB)	Initial HONO (PPB)	HC ^a initial (PPB)	Seed ^b	HC Consumed ^c (PPB)	Final OC (µg/m ³)	SOA yield ^d	Comments
C12A	07/08/22	Isododecane	911	100	220	None	76.5	0.7	0.001	Fig.2
C12B	06/07/22	N-dodecane	829	97	159	None	173.4	19.0	0.024	Madhu et al. (2023) Fig. 3
C12C	06/07/22	N-dodecane	331	200	135	None	131.3	123.2	0.206	Madhu et al. (2023) FTIR, Fig. 4
C15A	07/18/22	Trimethyldecane	936	140	220	None	162.0	103.8	0.110	Fig.2
C15B	08/04/22	Trimethyldecane	607	107	262	SA	161.6	141.2	0.150	Fig.2
C15C	02/17/22	N-pentadecane	665	117	202	None	125.3	117	0.285	Madhu et al. (2023) Fig. 3
C16A	09/02/22	Heptamethylnonane	433	80	170	None	60.0	3.5	0.006	Fig.2
C16B	09/02/22	Heptamethylnonane	205	60	160	None	63.0	1.7	0.003	Fig.2
C16C	04/14/23	Heptamethylnonane	120	90	100	AS	55.3	26.1	0.051	Fig.2
C16D	04/14/23	Heptamethylnonane	120	90	100	SA	60.6	25.7	0.046	Fig.2
C19A	07/29/22	Tetramethylpentadecane	260	110	195	None	147.7	447.5	0.276	Fig.2 FTIR, Fig. 4
C19B	08/09/22	Tetramethylpentadecane	251	100	163	SA	141.4	267.5	0.172	Fig.2 FTIR, Fig. 4
C19C	08/09/22	Tetramethylpentadecane	232	100	163	NS	140.1	389.7	0.253	Fig.2
C19D	03/30/23	Tetramethylpentadecane	229	39	39	NS	30.1	79.0	0.239	Fig.2
C19E	03/30/23	Tetramethylpentadecane	143	73	39	NS	36.1	149.6	0.377	Fig.2

^aInitial concentrations of Tetramethylpentadecane were calculated using a 95% injection efficiency as this compound is too low volatility to be measured by the GC-FID. ^bExperiments were performed with no seed (none) and sulfuric acid seed (SA). ^cValues for the amount of Tetramethylpentadecane consumed in each experiment are reported based on model simulations seen in Fig. S2 as this compound is too low volatility to be measured by the GC-FID. ^dYield was calculated as the ratio between the concentration of the final measured SOA mass (µg/m³) and the concentration of precursor alkane consumed (µg/m³).

125



130 **3 Model description**

The efficacy of the UNIPAR model has been demonstrated for simulating SOA formation from a variety of HC classes, including aromatic HCs (Im et al., 2014; Zhou et al., 2019; Han and Jang, 2022), monoterpenes (Yu et al., 2021b), and isoprene (Beardsley and Jang, 2016). In this study, UNIPAR model parameters were developed for the simulation of SOA formation from branched alkanes. The UNIPAR model simulates SOA mass formation via the multiphase reactions of HC precursors including gas (*g*), organic (*org*) and inorganic (*inorg*) phases. Typically, the UNIPAR model employs a near-explicit gas oxidation mechanism which is used to create a product distribution for each HC precursor by lumping products into an array consisting of 48 groups according to their volatility and reactivity. An approach using product structure-based lumping array renders the ability to simulate SOA formation via multiphase partitioning and in-particle chemistry that forms oligomeric products. In addition to SOA mass, SOA's chemical and physical characteristics, such as oxygen-to-carbon (O:C), aerosol viscosity, and functionality distributions, were simulated in the model. Detailed descriptions of lumping criteria and the mass-based stoichiometric coefficient (α_i) of lumping group *i* as a function of NO_x levels and the degree of aging can be found in previous studies (Madhu et al., 2023; Han and Jang, 2022; Choi and Jang, 2022; Yu et al., 2021b; Zhou et al., 2019). Because of a lack of practically applicable gas oxidation mechanisms for the variety of branched alkanes found in the atmosphere, a novel method was used to create lumping arrays for each branched alkane. Individual branched alkane lumping arrays were constructed primarily using existing lumping arrays, developed by Madhu et al. (2023), of the linear alkanes with the nearest vapor pressures. To account for the reduction of autoxidation products created by branched alkanes, an autoxidation reduction factor, which is a function of the degree and position of branching, was applied to lumping groups which contain autoxidation products. Figure 1 shows the UNIPAR model frame. In the presence of inorganic seed, the SOA mass is simulated via three paths: OM produced via multiphase partitioning of organic products (OM_P), aerosol phase reactions of organic species to form OM_{AR} via oligomerization in the *org* phase, and reactions in the wet *inorg* phase which also form OM_{AR} (acid-catalyzed oligomerization and organosulfate (OS) formation).

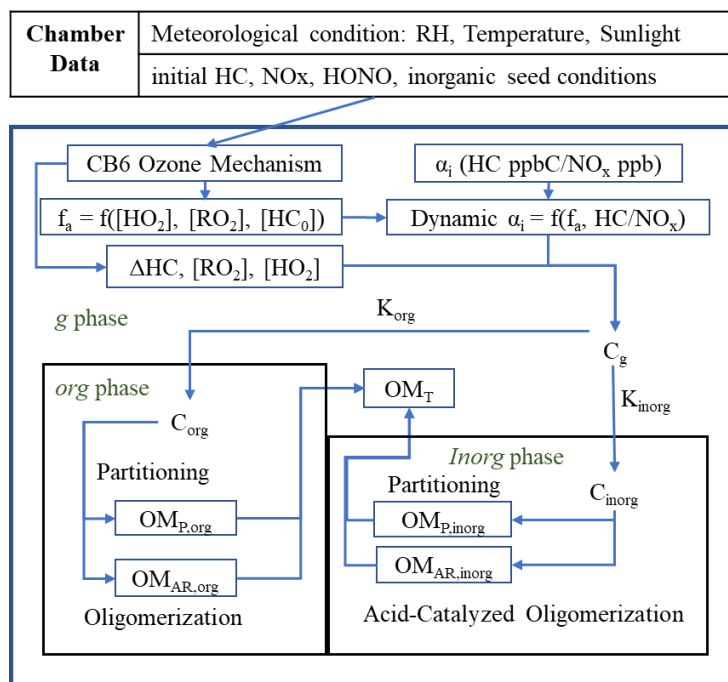


Figure 1. A simplified scheme of the UNIPAR model used in this study. $[HC]_0$ represents the initial hydrocarbon (HC) concentration. Chamber generated data is used to set initial conditions and the meteorological condition for the gas simulation. The CB6 Ozone mechanism is used to simulate the consumption of HC (ΔHC) and the concentrations of hydroperoxide radical ($[HO_2]$) and organic peroxy radical ($[RO_2]$). The dynamic mass-based stoichiometric coefficients (dynamic α_i) of lumping species i are calculated as a function of HC/ NO_x and the aging factor (f_a). f_a is represented as a function of $[HO_2]$, $[RO_2]$, and $[HC]_0$ (Zhou et al., 2019). The gas, organic, and inorganic phases are represented by the subscripts g , org , and $inorg$, respectively. K_{org} and K_{inorg} represent the partitioning coefficients of lumping species to the org phase and $inorg$ phase, respectively. C_{org} and C_{inorg} represent the concentrations of lumping species in the org and $inorg$ phases, respectively. $OM_{P,org}$ and $OM_{P,inorg}$ represent the mass of organic matter (OM) present in org and $inorg$ phases, respectively, due to partitioning. $OM_{Ar,org}$ and $OM_{Ar,inorg}$ represent the OM formed in the org phase due to in-particle chemistry such as oligomerization, and $inorg$ phase due to acid-catalyzed oligomerization and organosulfate formation (Beardsley and Jang, 2016; Im et al., 2014; Zhou et al., 2019). OM_T represents the total SOA mass formed.

165 3.1 UNIPAR model inputs

The parameter inputs to the UNIPAR model for each precursor HC include the equations for α_i and lumping species' physicochemical parameters, such as molecular weight (MW), O:C ratios, and hydrogen bonding (HB). The model inputs associated with each individual experiment include the consumption of HC (ΔHC); the concentrations of alkyl peroxide radical (RO_2) and hydroperoxyl radical (HO_2); concentrations of ionic species (sulfate and ammonium ions); temperature, and humidity. The measured sunlight profile for each experiment is linked to the gas oxidation of each HC yielding ΔHC ,



[RO₂], and [HO₂]. Gas simulation was performed in the box model platform of Dynamically Simple Model of Atmospheric Chemical Complexity (DSMACC) interfaced with the kinetic pre-processor (KPP). The predetermined mathematical equations for stoichiometric coefficients were constructed for linear alkanes by explicit gas mechanism as described in the following section 3.2. For the simulation of SOA mass, HC consumption of branched alkane was simulated with Carbon Bond 6 (CB6) mechanism.

3.2 Gas mechanisms

The atmospheric oxidation of alkanes begins with the reaction with an OH radical, followed by the addition of O₂ to form peroxy radicals. In the presence of NO_x, these peroxy radicals can form alkoxy radicals or organonitrate (Finlayson-Pitts and Pitts, 2000). In addition, peroxy radicals can create hydroperoxides via the reaction with HO₂ radicals. In the previous literature (Crouse et al., 2013; Bianchi et al., 2019; Roldin et al., 2019), the terpene peroxy radicals are capable of undergoing autoxidation reactions to form low volatility products. These reactions have been previously modeled (Pye Havala et al., 2019; Xavier et al., 2019). In the recent modelling study, Madhu et al. (2023), applies autoxidation mechanisms to improve the prediction of a series of linear alkane SOA. In their study, the product distribution of linear alkanes relatively in small carbon lengths (C₉-C₁₂) were predicted using explicit gas mechanisms which consisted of their respective Master Chemical Mechanism (MCM) and newly added autoxidation mechanisms. The product distributions, associated with stoichiometric coefficients, of lumping array were extrapolated to larger linear alkanes which do not currently have MCM mechanisms using an Incremental Volatility Coefficient (IVC). The feasibility of the lumping arrays generated with the IVC approach was demonstrated to predict chamber generated SOA data. For branched alkanes, explicit gas mechanisms are not currently available for the practical application to an SOA model. In this study, to produce product distributions for the variety of branched alkanes, the pre-existing linear alkane lumping arrays are extrapolated to branched alkanes as seen in section 3.4 below.

3.3 Lumping structure of UNIPAR model

As discussed in section 3.2, the lumping structure of branched alkane in the UNIPAR model is inherited from linear alkane. The lumping structure of the UNIPAR model, along with a dynamic α_i array which considers aging, has been developed in previous studies (Zhou et al., 2019; Han and Jang, 2020; Yu et al., 2021b). The lumping array is constructed based on products' volatility-reactivity characteristics. The α_i array consists of 6 different reactivity levels (very fast (VF), fast (F), medium (M), slow (S), partitioning only (P), and multi-alcohol (MA)) and 8 different volatility levels based on vapor pressure which represent 48 species. In the model, autoxidation products are typically allocated to low volatility, and low reactivity groups (volatility group 1 in reactivity groups P and S). Atmospheric aging can augment the product distribution, forming more reactive and less volatile products via oxidation, or photolysis products which are more volatile but may be more reactive. The stoichiometric coefficients of the lumping array are dynamically predicted as a function of NO_x and aging



as described in previous literature (Zhou et al., 2019; Han and Jang, 2020; Yu et al., 2021). A weighted aging factor is used to dynamically change α_i values based on fresh and highly oxidized compositions. The aging factor (f_a) at a time t , as detailed in Zhou et al. (2019), is defined as:

$$205 \quad f_a(t) = \log \frac{[HO_2] + [RO_2]}{[HC]_0} \quad (1)$$

where $[HO_2]$ and $[RO_2]$ and $[HC]_0$ are the concentrations of hydroperoxide radical, organic peroxy radical, and initial HC, respectively. Both fresh and highly oxidized lumping arrays are constructed for each NO_x level as well as the respective aging factors. $f_a(t)$ is also used to generate an aging scale that ranges from 0 (fresh composition) to 1 (highly oxidized composition) as follows (Zhou et al., 2019):

$$210 \quad f'_a(t) = \frac{f_a(\text{highly oxidized}) - f_a(t)}{f_a(\text{highly oxidized}) - f_a(\text{fresh})} \quad (2)$$

$f'_a(t)$ is calculated for a given NO_x level and used to dynamically calculate the α_i values for that same NO_x level as follows (Zhou et al., 2019):

$$\alpha_i = (1 - f'_a(t))(fresh \alpha_i) + (f'_a(t))(highly oxidized \alpha_i) \quad (3)$$

215 Physicochemical parameters of lumping species include MW, O:C ratio, and HB which are used to calculate multiphase partitioning and in-particle chemistry in the UNIPAR model. Further details about lumping criteria and physicochemical parameters can be found in the study by Zhou et al. (2019).

3.4 Construction of branched alkane lumping arrays

In the current UNIPAR model, the lumping arrays of a variety of linear alkanes can be predicted using the IVC approach (Madhu et al., 2023). To extend the lumping array of linear alkane to branched alkane, the volatility drop caused by branched alkyl groups was considered by matching each branched alkane to the linear alkane with the nearest vapor pressure. In addition, the lumping array in the model simulates the impact of the degree and position of branched alkyl groups on reducing the ability of branched alkanes to undergo autoxidation reactions. Figure S1 illustrates the ability of branched alkyl groups to reduce the ability of branched alkanes to undergo autoxidation reactions. For example, n-heptadecane has fourteen secondary carbons which can undergo autoxidation mechanism as seen in Fig. S1 (Left), while 2,2,4,4,6,8,8-
225 heptamethylnonane has only one secondary carbon which can process autoxidation due to the seven methyl branches which reduce the number of hydrogens available for abstraction. To account for this, an autoxidation reduction factor (ARF) is applied to the lumping array of branched alkane and calculated as follows:

$$ARF = \frac{AP \text{ of branched alkane}}{AP \text{ of linear alkane with nearest vapor pressure}} \quad (4)$$

230 where the autoxidation potential (AP) can be calculated as follows:

- a) Terminal carbons are not included for AP.



- b) Carbons that are adjacent to terminal carbons on the alkane backbone are assigned an AP value of 1 and this carbon can only undergo autoxidation reactions in one direction.
- c) Other carbons on the main alkane backbone are assigned an AP value of 2 due to the potential for autoxidation occurring in two directions.
- d) If 1 alkyl branch is present on a carbon, then the AP value is multiplied by 0.5.
- e) If geminal alkyl branches are present on a carbon, then the AP value is multiplied by 0.
- f) AP value of each alkane is the sum of all AP values for each carbon.

Table S1 summarizes the physical properties and ARF values for branched alkanes used in the chamber experiments of this study. Physicochemical parameters, and α -values of lumping arrays of compounds used for chamber experiments can be found in Sections S3 and S4. Ultimately, this approach allows for the reduction of SOA formation found in branched alkanes compared to that in linear alkanes with same carbon numbers.

3.5 SOA formation by multiphase partitioning

The partitioning process of lumping species is fundamental to form SOA and process in-particle chemistry. Partitioning coefficients for each lumping species, i , between g and org phase ($K_{or,i}$) or between the g and wet $inorg$ phase ($K_{in,i}$) are calculated using the typical gas-particle partitioning model (Pankow, 1994):

$$K_{or,i} = \frac{7.501RT}{10^9 MW_{org} \gamma_{org,i} p_{L,i}^0} \quad (5)$$

$$K_{in,i} = \frac{7.501RT}{10^9 MW_{inorg} \gamma_{inorg,i} p_{L,i}^0} \quad (6)$$

where R is the gas constant ($8.314 \text{ J mol}^{-1} \text{ K}^{-1}$), and T is temperature (K). MW_{org} and MW_{inorg} are the average molecular weights (g mol^{-1}) of the organic and inorganic phases of the aerosol, respectively. $p_{L,i}^0$ is the subcooled liquid vapor pressure of a species, i . The activity coefficient in or phase for each lumping species, $\gamma_{org,i}$, is assumed to be unity (Jang and Kamens, 1998). The activity coefficient in $inorg$ phase for each lumping species, $\gamma_{inorg,i}$, is predicted by a semi-empirical regression equation which was fit to the activity coefficients of various organic compounds as a function of physicochemical parameters (MW, O:C ratio, and HB) and sulfate fraction (FS). FS is an indicator for aerosol acidity which is defined as follows:

$$FS = \frac{[SO_4^{2-}]}{[SO_4^{2-}] + [NH_4^+]} \quad (7)$$

where $[SO_4^{2-}]$ and $[NH_4^+]$ are the concentration of sulfate and ammonium ions, respectively. The semi-empirical equation, derived from activity coefficients, estimated using the Aerosol Inorganic-Organic Mixtures Functional Groups Activity Coefficients (AIOMFAC) model (Zuend et al., 2011) at a given RH, is as follows:

$$\gamma_{inorg,i} = e^{0.035 \cdot MW_i - 2.704 \cdot \ln(\text{O:C}_i) - 1.121 \cdot \text{HB}_i - 0.330 \cdot \text{FS} - 0.022 \cdot (\text{RH})} \quad (8)$$

Further information on the derivation and statistical properties of Eq. (8) can be found in Zhou et al. (2019). The partitioning coefficients are used to calculate the concentration of each lumping species in the three phases ($C_{g,i}$, $C_{org,i}$, and $C_{inorg,i}$) from



the total concentration of each lumping species ($C_{T,i}$). The total SOA mass formed by partitioning (OM_P) in both *org* and *inorg* phases is predicted by the following equation which was developed by Schell et al. (2001) and reconstructed to consider mass formed by particle-phase reactions (OM_{AR}), seen in section 3.6, by Cao and Jang (2010):

$$265 \quad OM_P = \sum_i \left[C_{T,i} - OM_{AR,i} - C_{g,i}^* \frac{\frac{C_{org,i}}{MW_i}}{\sum_i \left(\frac{C_{org,i}}{MW_i} + \frac{OM_{AR,i}}{MW_{oli,i}} \right) + \frac{OM_0}{MW_{oli,i}}} \right] \quad (9)$$

where $C_{g,i}^*$ ($1/K_{org,i}$) and OM_0 (mol m^{-3}) represent the effective saturation concentration and pre-existing OM, respectively. $MW_{oli,i}$ and MW_i represent the molecular weights of oligomeric products and lumping species, respectively. Eq. (9) is solved using Newton-Rapson method, which iterates until a convergence is reached (Press et al., 1992).

3.6 SOA formation by particle-phase reactions

270 OM_{AR} is formed in both the *org* and *inorg* phases. In *org* phase, SOA formation is attributed to oligomerization as organic species undergo self-dimerization reactions (Han and Jang, 2020; Im et al., 2014; Yu et al., 2021; Zhou et al., 2019). In *inorg* phase, oligomerization of organic species can be accelerated by an acid catalyst (Jang et al., 2002). Oligomerization is expressed as a 2nd-order reaction (Odian, 2004) with rate constants $k_{AR,org,i}$ and $k_{AR,inorg,i}$ ($\text{L mol}^{-1} \text{s}^{-1}$) in *org* and *inorg* phases, respectively. $k_{AR,inorg,i}$ is described as follows:

$$275 \quad k_{AR,inorg,i} = 10^{0.25pK_{BH_i^+} + 1.0X + 0.95R_i + \log(a_w[H^+]) - 2.58} \quad (10)$$

where R_i represents species reactivity, $pK_{BH_i^+}$ represents the protonation equilibrium constant, a_w represents the activity of water, X represents excess acidity (Cox and Yates, 1979), and $[H^+]$ represents the concentration of protons which are estimated using the extended aerosol inorganic model (E-AIM (Clegg et al., 1998)) $k_{AR,org,i}$ is described as follows:

$$k_{AR,org,i} = 10^{[0.25pK_{BH_i^+} + 0.95R_i + 1.2 \left(1 - \frac{1}{1 + e^{0.005(300 - MW_{org})}} \right) + \frac{2.2}{1 + e^{6(0.75 - O:C)}} - 10.07]} \quad (11)$$

280 For the oligomerization in *org* phase, the terms related to acidity (X , and $a_w[H^+]$) are excluded. Studies have previously demonstrated that aerosol viscosity can influence the mobility of chemical species and thus, apparent reaction rates, which can be limited by slow bulk diffusion in the particle-phase (De Schrijver and Smets, 1966; Reid et al., 2018). The molecular weight of species in the organic phase (MW_{org}) and the O:C ratio, which are important predictors for viscosity, are considered to calculate $k_{AR,org,i}$ (Han and Jang, 2022).

285 Sulfuric acid can react with reactive organic compounds in the wet *inorg* phase of the aerosol to form dialkyl sulfate (diOS). The formed diOS can contribute to SOA mass production and also leads to a reduction in $[H^+]$ which decreases the rate of SOA mass produced by acid-catalyzed oligomerization in *inorg* phase. The formation of diOS is simulated in the UNIPAR model and reduces $[H^+]$ in *inorg* phase as previously reported (Im et al., 2014; Beardsley and Jang, 2016; Zhou et al., 2019).



3.7 Correction of intermediate organic vapor deposition to walls

290 Semi-volatile oxidized products derived from precursor HCs can deposit to chamber walls. As described in the previous studies by Han and Jang (2020), and Han and Jang (2022) the organic vapor deposition to wall is kinetically treated at the given chamber with the deposition ($k_{on,i}$) and desorption ($k_{off,i}$) rate constants of each lumping species, i . $k_{on,i}$ is expressed as a fractional loss rate (Mcmurry and Grosjean, 1985):

$$k_{on,i} = \left(\frac{A}{V}\right) \frac{\alpha_{w,i} \bar{v}_i / 4}{1 + \frac{\pi \alpha_{w,i} \bar{v}_i}{8(K_e D)^{1/2}}} \quad (12)$$

295 where D ($1.0 \times 10^{-6} \text{ m}^2 \text{ s}^{-1}$) and K_e (0.12 s^{-1}) are the diffusion coefficient and coefficient of eddy diffusion applied as a fixed number, respectively. $\left(\frac{A}{V}\right)$ represents the surface area to volume ratio of the chamber. \bar{v}_i and $\alpha_{w,i}$ represent the mean thermal speed of the gas molecules, and accommodation coefficient of i to the wall, respectively. Further information regarding the calculation of \bar{v}_i and $\alpha_{w,i}$ can be found a previous study (Madhu et al., 2023). $K_{w,i}$ ($K_{w,i} = k_{on,i}/k_{off,i}$) is calculated as follows:

$$300 \quad \ln(K_{w,i}) = -\ln(\gamma_{w,i}) - \ln(p_{L,i}^o) + \ln\left(\frac{7.501RTOM_{wall}}{10^9 MW_{OM}}\right) \quad (13)$$

OM_{wall} (mg m^{-3}) and MW_{OM} are the concentration of organic matter on the wall, and the molecular weight of organic matter on the wall, respectively. The activity coefficient ($\gamma_{w,i}$) of lumping species, i , in OM_{wall} is calculated using the quantitative structure-activity relationship (QSAR) approach with the physicochemical properties $H_{d,i}$, $H_{a,i}$, and P_i which represent hydrogen bond acidity, hydrogen bond basicity, and polarizability of each lumping group i , respectively (Abraham et al., 1991; Abraham and Mcgowan, 1987; Leahy et al., 1992; Platts et al., 1999; Puzyn et al., 2010). Eq. (13) can be rewritten as:

$$305 \quad \ln(K_{w,i}) = -(a_p H_{d,i} + b_p H_{a,i} + r_p P_i + c_p) - \ln(p_{L,i}^o) + \ln\left(\frac{7.501RTOM_{wall}}{10^9 MW_{OM}}\right) \quad (14)$$

The values of $H_{d,i}$, $H_{a,i}$, and P_i are calculated with the PaDEL-Descriptor, (Yap, 2011). The value of $K_{w,i}$ is used along with the $k_{on,i}$ to predict lumping species' wall loss using an analytical equation from the study by Han and Jang (2020) as follows:

$$C_{g,i} = \frac{K_{w,i} C_{T,i}}{K_{w,i} + 1} e^{-k_{on,i} \left(1 + \frac{1}{K_{w,i}}\right) t} + \frac{C_{T,i}}{K_{w,i} + 1} \quad (15)$$

310 where $C_{g,i}$ ($\mu\text{g m}^{-3}$) is the gas-phase concentration of a lumping species, i , after time step t (360 s). $C_{T,i}$ ($\mu\text{g m}^{-3}$) is the sum of $C_{g,i}$ and the concentration of lumping species i on the chamber wall ($C_{w,i}$ ($\mu\text{g m}^{-3}$)). The properties of gas-wall partitioning for branched alkanes were inherited from linear alkanes.

3.8 UNIPAR procedure for SOA mass production each time step

At each step, $C_{T,i}$ is estimated by using the newly produced ΔHC and α_i , and it is combined with the previous step's concentration of lumping species, except those used for the formation of OM_{AR} and organic vapor deposition to walls for the simulation of chamber data. Then, the updated $C_{T,i}$ is applied to generate $C_{g,i}$, $C_{org,i}$, and $C_{inorg,i}$ based on multiphase

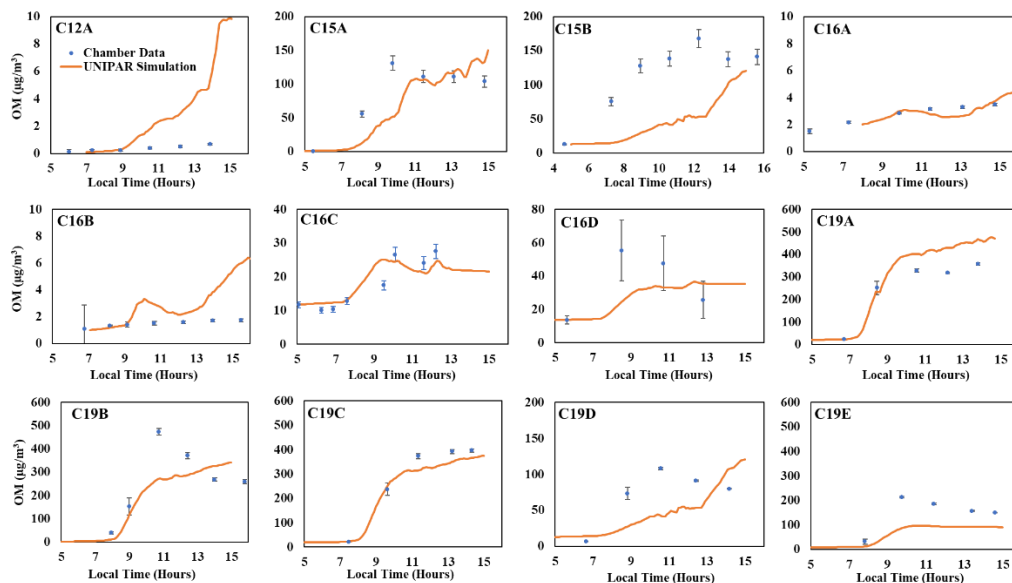


partitioning coefficients as seen in Eq. (5) and Eq. (6). C_{inorg} and C_{org} are then used to form OM_{AR} via oligomerization in both the *inorg* and *org* phases with the rate constants calculated in Eq. (10) and Eq. (11), respectively. In the model, the quantity of the sulfate associated with OS in the *inorg* phase is also estimated and applied to recalculate $[H^+]$. After the process to form OM_{AR} , the remaining concentration of lumping species is used to estimate the organic vapor deposition to the wall using Eq. (15). OM_P is calculated using a Newtonian approach (Eq. 9) in the presence of OM_{AR} and the preexisting OM_0 at the end of each time step. For the total SOA mass, OM_{AR} , OM_P and OM_0 are combined.

4 Results and Discussion

4.1 Chamber data vs. model prediction

The feasibility of the UNIPAR model to predict the SOA formation from various branched alkanes (Table S1) was demonstrated by comparing simulations with chamber data collected under various experimental conditions in the UF-APHOR chamber. As seen in Fig. 2, the UNIPAR model is reasonably able to predict the SOA formation from 2,6,10-Trimethyldodecane (C15), 2,2,4,4,6,8,8-Heptamethylnonane (C16), and 2,6,10,14-Tetramethylpentadecane (C19) at both high and low NO_x conditions under different seed conditions (Table 1). Gas simulations used to predict HC consumption, RO_2 concentrations, and HO_2 concentrations performed using the CB6 mechanism can be seen in Fig. S2. As seen in the gas simulation, consumption of Isododecane was overpredicted compared to chamber measurements. This is likely due to the relatively low purity (80%) of commercially available Isododecane that was used for the chamber experiment. However, even with an overprediction for the gas consumption, the UNIPAR model SOA showed only a slight overprediction, indicating that the relatively low SOA yield of Isododecane is well represented within the model.



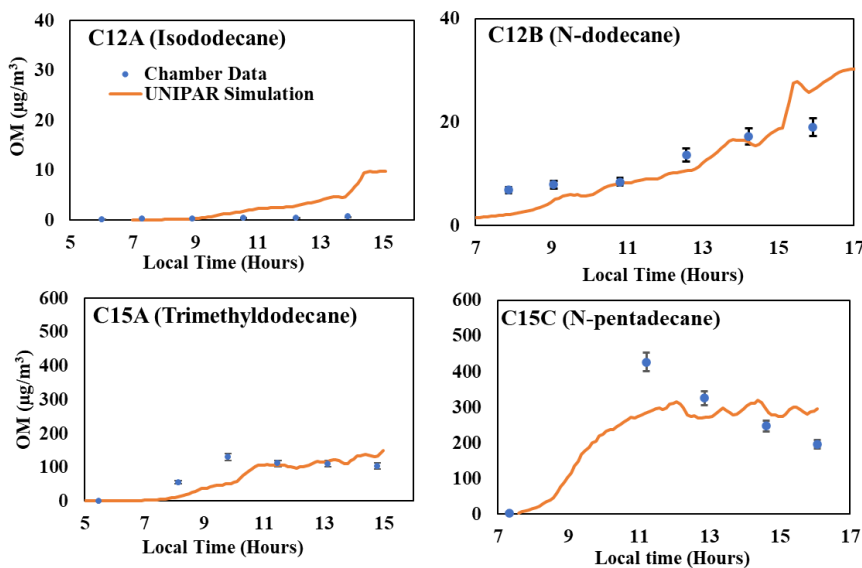
335

Figure 2. Comparison of SOA mass produced between simulations for Isododecane, Trimethyldodecane, Heptamethylnonane, and Tetramethylpentadecane to chamber data (Table 1). The blue dots represent observed SOA data collected that are corrected for particle wall loss to the chamber. Error bars represent a 95% confidence interval for each data point.

340

Generally, the presence of branching significantly reduced the amount of alkane SOA mass. This impact can be seen when comparing chamber data generated for Isododecane (branched C12) to linear C12 and chamber data generated for Trimethyldodecane (branched C15) to linear C15 as seen in Fig.3. Remarkably, highly branched C16 (Fig. 2) shows a lower capability for SOA formation compared to linear C15 (Fig. 3). Overall, the typical impact of NO_x levels on SOA formation appeared, showing a negative relationship. Unlike SOA generated from aromatics (Im et al., 2014), branched alkane SOA was insensitive to seed condition due to the low polarity of the products. A similar result is observed in linear alkane SOA reported by Madhu et al. (2023). Further discussion on the impact of alkyl branches, NO_x conditions, humidity, seed, and temperature can be found in the upcoming sections 4.3 and 4.4.

345



350

Figure 3. Comparison of the SOA mass produced by two branched alkanes (Isododecane and Trimethyldecane) to the mass produced by linear alkanes (Madhu et al., 2023) of the same carbon number (Table 1). Error bars for C12A and C15A represent a 95% confidence interval for each data point. Error bars for C12B and C15C are 8% as reported by Madhu et al. (2023).

355 4.2 Characterization of aerosol composition

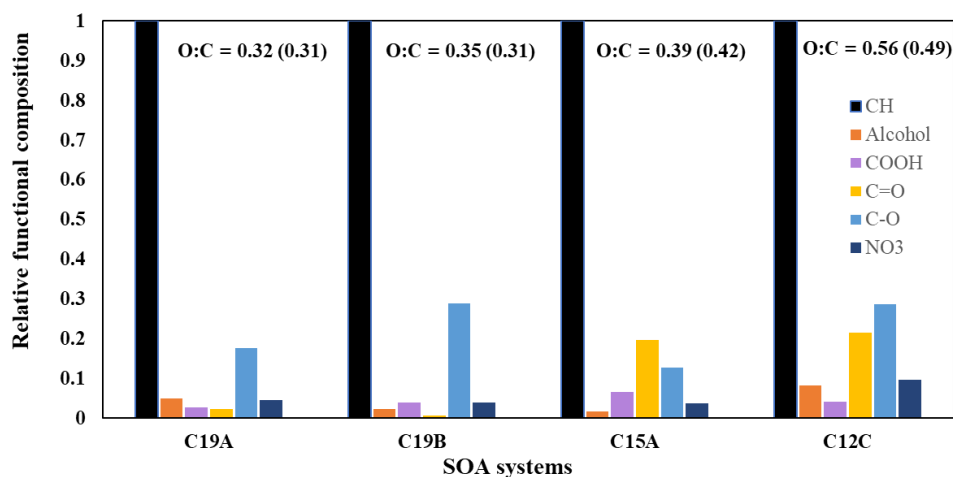
Figure 4 displays the relative functional group compositions of various alkane SOA constructed using FTIR data. FTIR spectra were decoupled into functional groups using the curve fitting method, assuming that a Gaussian distribution governs each peak. The decoupled FTIR bend for each functional group was applied to estimate the functionality composition of alkane aerosol using the relative intensity of the functional group determined from various reference compounds. The fitting parameters are the center frequency, the peak absorbance, and the half width at half-height. The relative functional group intensities for –OH, –COOH, C=O in ketones and aldehydes, C–O in non-alcohol and non-carboxylic acid groups, and NO₃ in organonitrates were normalized with that of C–H stretching. The O:C ratios, calculated using functional group distributions from FTIR spectra, are also shown in Fig. 4 alongside model predicted O:C ratios. The model is able to reasonably predict O:C ratios for chamber generated data for both branched and linear alkanes. As expected, alkanes with a larger number of carbons tend to produce less oxidized SOA compared to alkanes with a smaller number of carbons. The relatively low O:C ratios found in alkane SOA systems support our assumption that organic and wet inorganic phases exist separately as most organic species are unlikely to be soluble in the inorganic phase (Yu et al., 2021a). When comparing the SA-seeded C19 and non-seeded C19 SOA systems, the SA system shows smaller amount of C=O functional groups but

360

365



370 higher amount of C-O, evidently indicating some acid-catalyzed oligomerization, although the impact of wet inorganic seed is small (section 4.4). All SOA systems shown in Fig. 4 are produced under relatively low NO_x conditions (Table 1). Increasing the NO_x levels during alkane oxidation may increase the amount of nitrate functional groups in SOA.



375 Figure 4. Relative functional group compositions of different SOA systems constructed using FTIR data. The O:C ratios of each SOA system, constructed with the functional group composition from FTIR data, are shown along with model-predicted O:C ratios displayed in parentheses.

4.3 Sensitivity of alkane SOA yields to alkyl branches

380 Figure 5 illustrates the impact of alkyl branches on the SOA Yields of an alkane with 15 carbons. Information on the structures, parameters used to generate lumping arrays, and calculated OH-radical reaction rates for alkanes used in Fig. 5 can be found in Table S4. Figure 5 clearly demonstrates the decrease in alkane SOA yields as the number of alkyl branches increases at given oxidation conditions. This figure also illustrates the relative importance of the ARF in the model compared to the vapor pressure drop due to branching. When the number of branches increases, the decrease in vapor pressure may not be large enough such that the linear alkane with the nearest vapor pressure changes. For example, C15 alkanes with one branch and two branches, at the given structures, both have vapor pressures nearest to that of linear C14 (Table S4). In this case, the ARF becomes the only method to decrease SOA yields and the decrease in SOA yields due to an increase in alkyl branches is relatively small within the model. Additionally, when comparing the C15 alkane with one branch to the one with two branches, the difference in SOA yields for the low NO_x condition is slightly larger when compared to the difference in SOA yields for the high NO_x condition. This indicates that, similarly to linear alkanes (Madhu et al., 2023), the fraction of branched alkane autoxidation products of total SOA mass in low NO_x conditions is larger compared to that in high NO_x conditions. Further discussion on the impact of NO_x conditions on the SOA yields of branched alkanes can be found in the upcoming section 4.4.

390

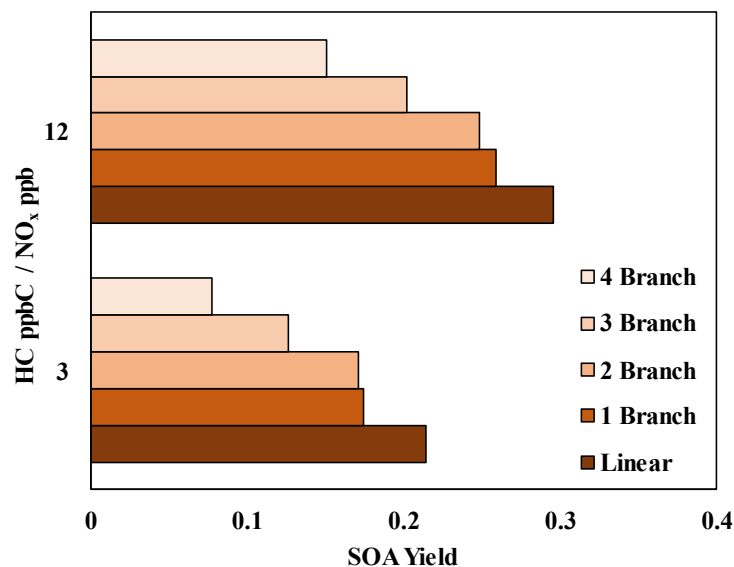


Figure 5. Simulated SOA Yields for 15 carbon alkanes with various number of branches at two different NO_x levels. OM₀ = 5 μg/m³, 298 K, RH = 60%, HC consumption = 100 μg/m³, sunlight profile shown in Fig. S3.

4.4 Sensitivity of branched alkane SOA formation to NO_x levels, temperature, humidity, and seed conditions

395 Figure 6 illustrates the SOA yields of three alkanes that each have 3 branched methyl groups (C12, C15, C18) under various NO_x levels. Information on the structures, parameters used to generate lumping arrays, and calculated OH-radical reaction rates for alkanes used in Fig. 6 can be found in Table S5. Similarly to most SOA precursors, the simulated SOA yields of all three branched alkanes increased as NO_x levels decreased. Because gas simulations are conducted in a manner which the HC consumption is kept fixed for each condition, the difference between SOA yields at different NO_x levels can be attributed to a change in product distributions. In high NO_x conditions, the paths to form organonitrate products can compete with the paths which form low-volatility products via autoxidation. In addition, the formation of organonitrate suppresses the further oxidation of products. Less oxidized products tend to be less volatile products which reduce SOA yields.

400

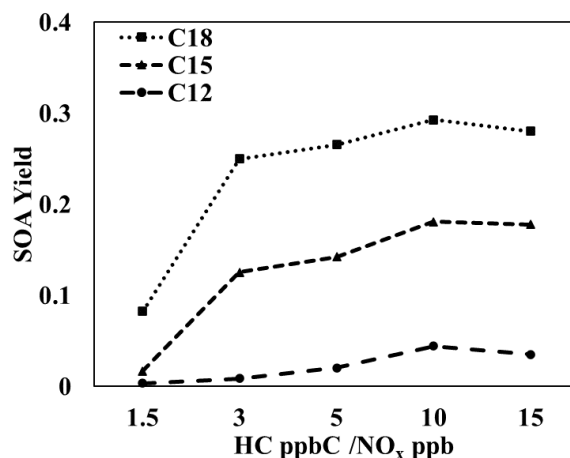


Figure 6. Simulated SOA yields for three-branched alkanes of different carbon numbers (C12, C15, C18) at various HC ppbC/NO_x ppb levels. OM₀ = 5 μg/m³, 298 K, RH = 60%, HC consumption = 100 μg/m³, sunlight profile shown in Fig. S3.

Figure 7 illustrates the SOA yields of 2,6,10-Trimethyldecane under 3 different seed conditions (ammonium sulfate (AS), sulfuric acid (SA), and no seed (NS)) and two RH conditions (30% and 60%). Under 60% RH, the AS seed is wet, and under 30% RH, the AS seed is dry. Similarly to linear alkanes (Madhu et al. 2023), branched alkanes SOA yields were not significantly impacted by the presence of seed under either humidity condition. Additionally, no significant impact of acidic seed on branched alkane appeared, indicating that alkane SOA formation is dominated by partitioning rather than particle phase chemistry. This is consistent with the FTIR data (Fig. 4) which shows a lack of reactive aldehydic C=O species which can be involved in acid-catalyzed oligomerization.

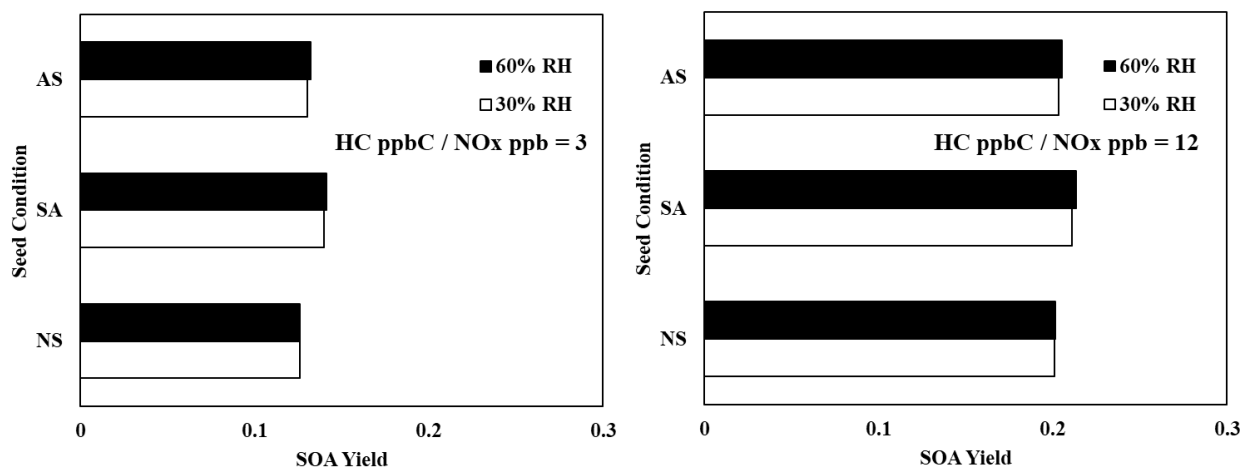


Figure 7. Simulated SOA Yields for 2,6,10-Trimethyldecane at various seed conditions (10 μg/m³ Ammonium Sulfate (AS), 10 μg/m³ Sulfuric Acid (SA), and no seed (NS)) and 2 HC ppbC / NO_x ppb levels. OM₀ = 5 μg/m³, 298 K, RH = 60%, HC consumption = 100 μg/m³, sunlight profile shown in Fig. S3.



Figure 8 displays the SOA yields of three different 3-branched alkanes (Table S5) under 3 different temperatures and two
 420 different NO_x conditions. As expected, due to the relatively high importance of partitioning, the SOA yields of all the 3-
 branched alkanes are significantly impacted by changes in temperature under both NO_x conditions. Additionally, the impact
 of temperature on SOA yields decreases as the number of carbons increase because larger molecules typically produce more
 low-volatility products which tend to exist in the particle-phase at various temperatures. Generally, the SOA produced at low
 NO_x levels is less sensitive to temperature due to the larger contribution of low-volatility products via autoxidation.
 425 A similar tendency was previously reported for linear alkanes (Madhu et al., 2023).

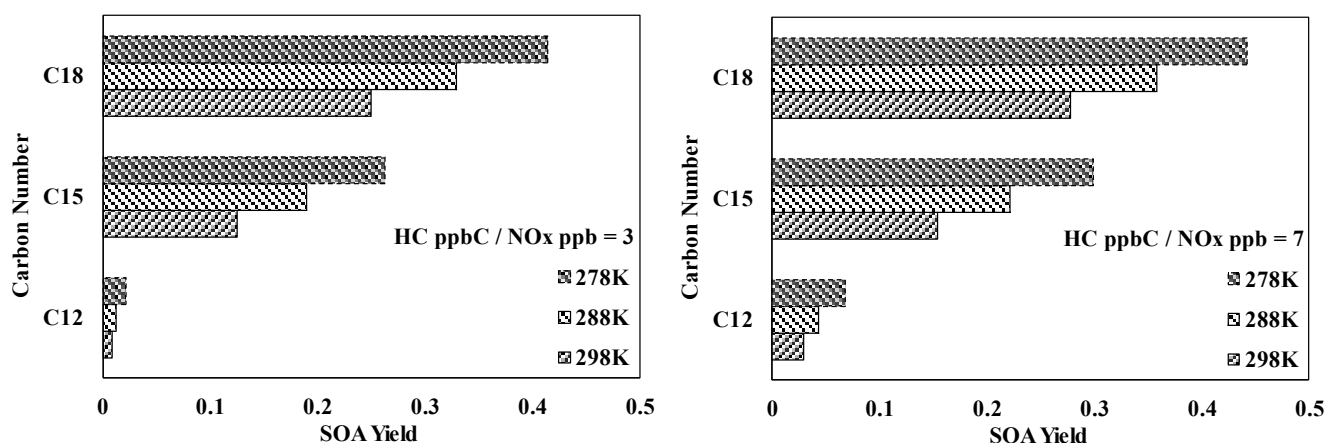
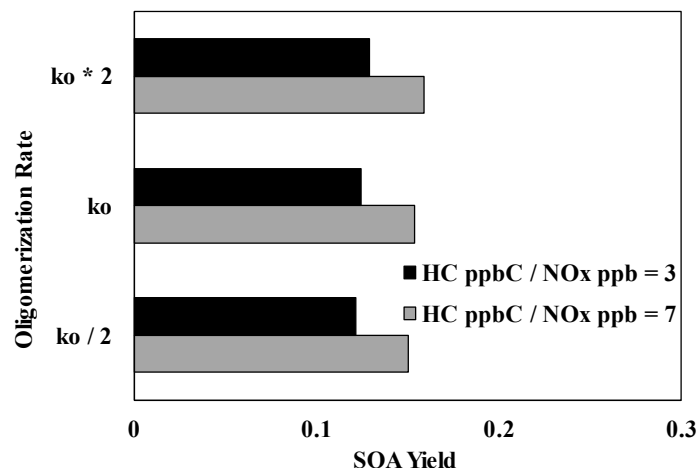


Figure 8. Simulated SOA Yields from photooxidation of three different 3-branched alkanes (Table S3) at three different
 temperatures (278K, 288K, 298K) and two different NO_x levels (HC ppbC/ NO_x ppb = 3, 7). $\text{OM}_0 = 5 \mu\text{g}/\text{m}^3$, $\text{RH} = 60\%$, HC
 430 consumption = $100 \mu\text{g}/\text{m}^3$, sunlight profile shown in Fig. S3.

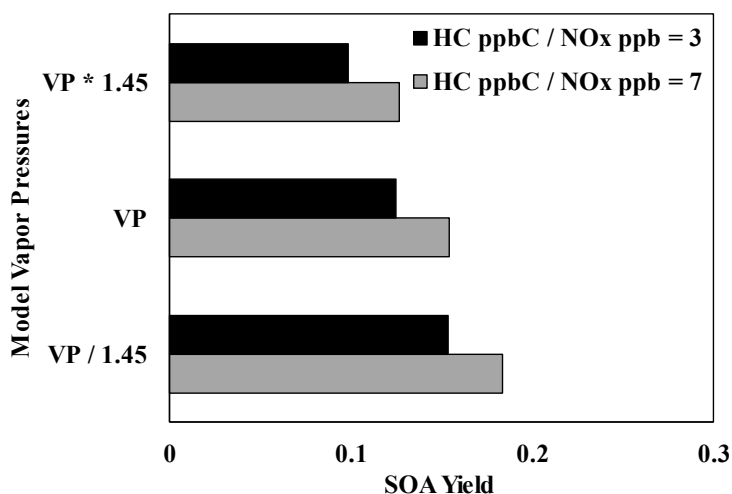
4.5 Uncertainty of model rate constants

Figure 9 illustrates the impact of increasing and decreasing the UNIPAR oligomerization rate constant by a factor of 2 on the
 SOA yields of 2,6,10-Trimethyldeodecane at both high and low NO_x levels. Unlike aromatic SOA (Im et al., 2014; Zhou et
 al., 2019; Han and Jang, 2022), the SOA yields were not significantly impacted by either change to the oligomerization rate
 435 constant under both NO_x conditions. This reaffirms the previously discussed (Sections 4.2, 4.4) idea that particle-phase
 reactions serve a relatively small part in branched alkane SOA formation due to the lack of reactive oxidation products.
 Thus, within this model, there is a low level of uncertainty which originates from the rate constant for particle phase
 reactions.



440 Figure 9. Impact of increasing and decreasing the UNIPAR oligomerization rate constant by a factor of 2 on the SOA yields of 2,6,10-Trimethyldodecane at two different NO_x levels (HC ppbC / NO_x ppb = 3, 7). OM₀ = 5 µg/m³, RH = 60%, HC consumption = 100 µg/m³, sunlight profile shown in Fig. S3.

Vapor pressures related to volatility groups were calculated using a group contribution method that has an estimated uncertainty of a factor of 1.45 (Zhao et al., 1999; Myrdal and Yalkowsky, 1997). Fig. 10 displays the impact of uncertainties in the estimation of vapor pressure in UNIPAR. Contrary to the oligomerization rate constant, changing the lumping group vapor pressures causes significant changes in SOA yield which demonstrates the important role of partitioning in branched alkane SOA formation.



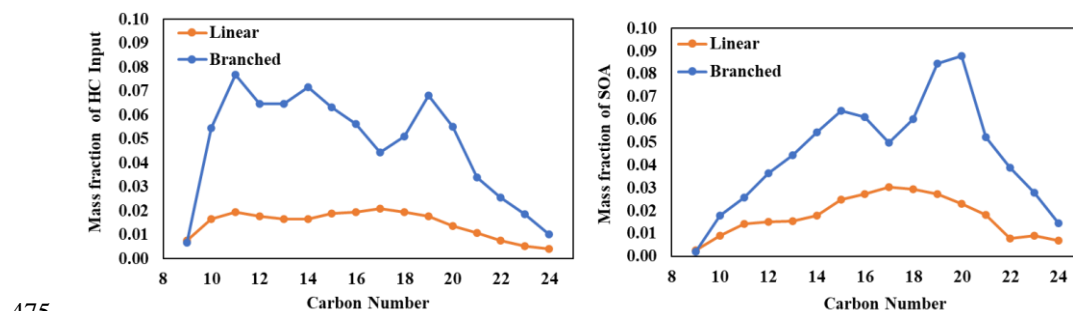
450 Figure 10. Impact of increasing/decreasing the UNIPAR lumping group vapor pressures by a factor of 1.45 on the SOA yields of 2,6,10-Trimethyldodecane at two different NO_x levels (HC ppbC / NO_x ppb = 3, 7). OM₀ = 5 µg/m³, RH = 60%, HC consumption = 100 µg/m³, sunlight profile shown in Fig. S3



4.6 Application of IVC-base product distributions to SOA simulation from diesel linear and branched alkanes

455 Diesel fuel is comprised of various linear and branched alkanes dominantly ranging from C9 to C24. The composition of linear and branched alkanes in diesel fuel, reported by Genter et al. (2012), was applied to the UNIPAR model in Fig. 11. The gas simulation of diesel fuel was performed using the CB6 Ozone mechanism with relative concentrations of diesel fuel linear and branched alkanes (100 $\mu\text{g}/\text{m}^3$ total), as well as other common diesel constituents, as reported by Sazhin et al. (2014), under urban conditions (high NO_x level). SOA formation was simulated only from branched and linear alkanes but the inclusion other diesel constituents allows for more accurate predictions of concentrations RO_2 and HO_2 , as well as individual HC consumptions. Each branched alkane was assumed to have 3 methyl branches. Within the UNIPAR model, SOA formation from all linear and branched alkanes was performed simultaneously, such that the SOA mass formed from one precursor can enhance the SOA mass formed from every other precursor. As seen in Fig.1, branched alkanes represent a higher proportion of diesel fuel and also SOA mass formed compared to linear alkanes. Branched alkanes represented 78% of the alkane HC input and were responsible for 72% of the total SOA mass produced.

465 Additionally, long-chain alkanes ($\geq \text{C}15$) are relatively more important for SOA formation compared to smaller alkanes within both the linear and branched subsets. Long-chain linear alkanes represented 59% of the linear alkane composition in diesel and was responsible for 73% of the total linear alkane SOA mass production. Similarly, long-chain branched alkanes represented 56% of the branched alkane composition in diesel fuel and was responsible for 75% of the total branched alkane SOA mass production. Our conclusion regarding the importance of long-chain alkanes generally agrees with the conclusion presented by Madhu et al. (2023). However, the linear alkane SOA formation simulation by Madhu et al. (2023) was performed individually for each precursor, which did not allow for SOA mass produced from one precursor to influence the others. Thus, Fig. 11 is a better representation of the SOA formation potential from linear and branched alkanes in diesel fuel. However, the inclusion of other diesel constituents (e.g., cyclic alkanes, polyaromatics HCs, and aromatics) may further augment the SOA formation potential of the various linear and branched alkanes diesel fuel (Gentner et al., 2012).



475 Figure 11. SOA formation from the photooxidation of diesel fuel linear and branched alkanes in the presence of NO_x . Composition as reported by Gentner et al. (2012). Concentration of initial HC = 993 ppbC, temperature = 298 K, RH = 60%, and HC ppbC/ NO_x ppb = 3, sunlight profile shown in Fig. S3.



4.7 Summary and Conclusions

480 Branched alkanes are one of the major classes of HCs in urban environments, specifically representing significant
proportions of both gasoline and diesel fuel (Gentner et al., 2012). Unlike aromatics, alkanes can be sourced both
anthropogenically and biogenically and thus, they are likely to remain as important precursors even after fossil fuel usage
decreases. This study models SOA formation using the UNIPAR model via the multiphase reactions of branched alkanes.
Due to a lack of practically applicable gas mechanisms available for a variety of branched alkanes, the lumping arrays of
485 branched alkanes were predicted using previously existing lumping arrays of linear alkanes. To do so, the lumping array of
each branched alkane was primarily created using the lumping array of the linear alkane with the nearest vapor pressure. In
addition to a decrease in vapor pressure, branching present on an alkane chain can reduce the ability of the oxidation
products to undergo autoxidation (Fig. S1). Autoxidation has been demonstrated in previous studies which show that
autoxidation products significantly contribute to terpene SOA (Pye et al., 2019; Xavier et al., 2019; Yu et al., 2021), and
490 linear alkane SOA (Madhu et al., 2023). To account for the reduction of autoxidation products in branched alkane compared
to that in linear alkanes, an ARF value (Eq. 4) was applied to the α -values of lumping groups. Lumping arrays generated in
this manner were applied within UNIPAR to predict SOA formation from branched alkanes, which was compared to
chamber data. The model predicted SOA formation well agreed with chamber data (Fig. 2). Additionally, O:C values of
chamber generated SOA, which were calculated using FTIR spectra, also were in agreement with model predicted O:C
495 values.

Similarly to linear alkanes (Madhu et al., 2023), branched alkanes showed significant sensitivity to NO_x levels as seen in Fig.
6. The degree of branching was also shown to significantly impact branched alkane SOA, with yields generally decreasing as
the number of methyl branches increases (Fig. 5). As branching increases, the vapor pressure increase of the precursor and
subsequent oxidation products was determined to a more significant factor contributing to branched alkane SOA yields than
500 the ARF (section 4.3). The branched alkane SOA formation is dominated by gas-particle partitioning processes, particularly
between the gas and organic phases due to the relatively non-polar oxidation products. Evidently, SOA yields are sensitive to
temperature (Fig. 8), an environmental factor that is heavily tied to partitioning. Furthermore, branched alkane SOA yields
are insensitive to changes in particle-phase reaction rates (Fig. 9) and show no significant impacts from changes in aerosol
acidity or inorganic seed composition (Fig. 7).

505 The conclusions presented have several real-world implications. Firstly, branched alkanes are significant sources of SOA
formation and should be considered as an SOA precursor, especially in urban environments where vehicular emissions
represent a significant proportion of the emitted reactive organic carbon (Murphy et al., 2023). As shown in Fig. 11,
branched alkanes within diesel were responsible for a significantly larger proportion of SOA mass production compared to
linear alkanes. Secondly, the reduction of NO_x concentrations in the atmosphere would not be effective to decrease branched
510 alkane SOA formation as branched alkane SOA yields tend to increase as NO_x levels decrease (Fig. 6). Thirdly, branched
alkane SOA yields would not be significantly affected by the reduction of sulfate because of relatively non-polar, non-



reactive oxidative products (Section 4.4).

The branched alkane SOA prediction using the UNIPAR model contains several sources of uncertainty. As previously explained, the UNIPAR parameters of each branched alkane were primarily inherited from an analogous linear alkane. For example, vapor pressures of precursor branched alkanes were matched with the linear alkane with the nearest vapor pressure. However, the two matched vapor pressures are rarely identical, and this deviation between the two values can yield uncertainty in the predicted lumping array. Similarly, physicochemical parameters (e.g. O:C, HB, and MW arrays, and wall loss parameters) inherited from linear alkanes can be included as sources of uncertainty in SOA prediction. Additionally, the branched alkane lumping arrays also inherited uncertainty associated with the linear alkane oxidation mechanisms that were originally used to generate linear alkane lumping arrays. As described by Madhu et al. (2023), the linear alkane gas oxidation mechanisms used to generate lumping arrays were written in such a way that, if a precursor has several possible points of reaction with a hydroxyl radical, only one path is included. The inclusion of alternative pathways may augment the linear alkane lumping arrays and have downstream effects on branched alkane lumping arrays.

In this study, SOA formation from the photooxidation of linear and branched alkanes in diesel fuel was predicted by using UNIPAR model. However, diesel fuels also contain significant amounts of cyclic alkanes, which tend to have higher propensities to be SOA precursors (Manavi and Pandis, 2022). When considering SOA formation from alkanes in diesel, cyclic alkanes should be included to accurately predict SOA formation potentials.

Code availability

Code to run the SOA model in this study is available upon request.

Data availability

The chamber data and simulated results used in this study are available upon request.

Author contributions

MJ designed the experiments, and AM and MJ carried them out. AM prepared the manuscript with contributions from MJ and YJ.

Competing interests

The authors declare that they have no conflict of interest.

Financial Support

This research was supported by the National Institute of Environmental Research (NIER2021); the National Science Foundation (AGS1923651); and the Fine Particle Research Initiative in East Asia Considering National Differences

<https://doi.org/10.5194/egusphere-2023-1500>

Preprint. Discussion started: 28 August 2023

© Author(s) 2023. CC BY 4.0 License.



545 (FRIEND) Project through the National Research Foundation of Korea (NRF) funded by the Ministry of Science and ICT (2020M3G1A1114556)



References

- Abraham, M. H. and McGowan, J. C.: The Use of Characteristic Volumes to Measure Cavity Terms in Reversed Phase
550 Liquid Chromatography, *Chromatographia*, 23, 243-246, 1987.
- Abraham, M. H., Whiting, G. S., Doherty, R. M., and Shuely, W. J.: Hydrogen bonding: XVI. A new solute salvation parameter, π_2H , from gas chromatographic data, *Journal of Chromatography A*, 587, 213-228, [https://doi.org/10.1016/0021-9673\(91\)85158-C](https://doi.org/10.1016/0021-9673(91)85158-C), 1991.
- Alves, C., Vicente, A., Pio, C., Kiss, G., Hoffer, A., Decesari, S., Prevôt, A. S. H., Minguillón, M. C., Querol, X., Hillamo, R., Spindler, G., and Swietlicki, E.: Organic compounds in aerosols from selected European sites – Biogenic versus anthropogenic sources, *Atmospheric Environment*, 59, 243-255, <https://doi.org/10.1016/j.atmosenv.2012.06.013>, 2012.
- Aumont, B., Camredon, M., Mouchel-Vallon, C., La, S., Ouzebidou, F., Valorso, R., Lee-Taylor, J., and Madronich, S.: Modeling the influence of alkane molecular structure on secondary organic aerosol formation, *Royal Society of Chemistry*, 165, 105-122, 2013.
- 560 Beardsley, R. L. and Jang, M.: Simulating the SOA formation of isoprene from partitioning and aerosol phase reactions in the presence of inorganics, *Atmos. Chem. Phys.*, 16, 5993-6009, 10.5194/acp-16-5993-2016, 2016.
- Bianchi, F., Kurtén, T., Riva, M., Mohr, C., Rissanen, M. P., Roldin, P., Berndt, T., Crouse, J. D., Wennberg, P. O., Mentel, T. F., Wildt, J., Junninen, H., Jokinen, T., Kulmala, M., Worsnop, D. R., Thornton, J. A., Donahue, N., Kjaergaard, H. G., and Ehn, M.: Highly Oxygenated Organic Molecules (HOM) from Gas-Phase Autoxidation Involving Peroxy Radicals: A
565 Key Contributor to Atmospheric Aerosol, *Chemical Reviews*, 119, 3472-3509, 10.1021/acs.chemrev.8b00395, 2019.
- Cao, G. and Jang, M.: An SOA Model for Toluene Oxidation in the Presence of Inorganic Aerosols, *Environmental Science & Technology*, 44, 727-733, 10.1021/es901682r, 2010.
- Caplain, I., Cazier, F., Nouali, H., Mercier, A., Déchaux, J.-C., Nollet, V., Joumard, R., André, J.-M., and Vidon, R.: Emissions of unregulated pollutants from European gasoline and diesel passenger cars, *Atmospheric Environment*, 40, 5954-5966, <https://doi.org/10.1016/j.atmosenv.2005.12.049>, 2006.
- 570 Choi, J. and Jang, M.: Suppression of the phenolic SOA formation in the presence of electrolytic inorganic seed, *Science of The Total Environment*, 851, 158082, <https://doi.org/10.1016/j.scitotenv.2022.158082>, 2022.
- Clegg, S. L., Brimblecombe, P., and Wexler, A. S.: Thermodynamic Model of the System $H^+-NH_4^+-SO_4^{2-}-NO_3^- -H_2O$ at Tropospheric Temperatures, *The Journal of Physical Chemistry A*, 102, 2137-2154, 10.1021/jp973042r, 1998.
- 575 Cox, R. A. and Yates, K.: Kinetic equations for reactions in concentrated aqueous acids based on the concept of "excess acidity", *Canadian Journal of Chemistry*, 57, 2944-2951, 10.1139/v79-479, 1979.
- Crouse, J. D., Nielsen, L. B., Jørgensen, S., Kjaergaard, H. G., and Wennberg, P. O.: Autoxidation of Organic Compounds in the Atmosphere, *The Journal of Physical Chemistry Letters*, 4, 3513-3520, 10.1021/jz4019207, 2013.
- De Schrijver, F. and Smets, G.: Polymerization kinetics in highly viscous media, *Journal of Polymer Science Part A-1: Polymer Chemistry*, 4, 2201-2210, <https://doi.org/10.1002/pol.1966.150040914>, 1966.
- 580 EPA, U. S.: U.S. EPA. Integrated Science Assessment (ISA) for Particulate Matter 2019.
- Finlayson-Pitts, B. J. and Pitts, J. N.: CHAPTER 4 - Photochemistry of Important Atmospheric Species, in: *Chemistry of the Upper and Lower Atmosphere*, edited by: Finlayson-Pitts, B. J., and Pitts, J. N., Academic Press, San Diego, 86-129, <https://doi.org/10.1016/B978-012257060-5/50006-X>, 2000.
- 585 Gentner, R., Isaacman, G., Worton David, R., Chan Arthur, W. H., Dallmann Timothy, R., Davis, L., Liu, S., Day Douglas, A., Russell Lynn, M., Wilson Kevin, R., Weber, R., Guha, A., Harley Robert, A., and Goldstein Allen, H.: Elucidating secondary organic aerosol from diesel and gasoline vehicles through detailed characterization of organic carbon emissions, *Proceedings of the National Academy of Sciences*, 109, 18318-18323, 10.1073/pnas.1212272109, 2012.
- Han, S. and Jang, M.: Simulating the impact of gas-wall partitioning on SOA formation using the explicit gas mechanism integrated with aqueous reactions containing electrolytes, *Science of The Total Environment*, 748, 141360, <https://doi.org/10.1016/j.scitotenv.2020.141360>, 2020.
- 590 Han, S. and Jang, M.: Prediction of secondary organic aerosol from the multiphase reaction of gasoline vapor by using volatility-reactivity base lumping, *Atmos. Chem. Phys.*, 22, 625-639, 10.5194/acp-22-625-2022, 2022.
- Im, Y., Jang, M., and Beardsley, R. L.: Simulation of aromatic SOA formation using the lumping model integrated with explicit gas-phase kinetic mechanisms and aerosol-phase reactions, *Atmos. Chem. Phys.*, 14, 4013-4027, 10.5194/acp-14-4013-2014, 2014.
- 595



- Jang, M. and Kamens, R. M.: A Thermodynamic Approach for Modeling Partitioning of Semivolatile Organic Compounds on Atmospheric Particulate Matter: Humidity Effects, *Environmental Science & Technology*, 32, 1237-1243, 10.1021/es970773w, 1998.
- 600 Jang, M., Czoschke, N. M., Lee, S., and Kamens, R. M.: Heterogeneous Atmospheric Aerosol Production by Acid-Catalyzed Particle-Phase Reactions, *Science*, 298, 814-817, doi:10.1126/science.1075798, 2002.
- Jo, Y., Jang, M., Han, S., Madhu, A., Koo, B., Jia, Y., Yu, Z., Kim, S., and Park, J.: CAMx-UNIPAR Simulation of SOA Mass Formed from Multiphase Reactions of Hydrocarbons under the Central Valley Urban Atmospheres of California, *EGUsphere*, 2023, 1-30, 10.5194/egusphere-2023-93, 2023.
- 605 La, Y. S., Camredon, M., Ziemann, P. J., Valorso, R., Matsunaga, A., Lannuque, V., Lee-Taylor, J., Hodzic, A., Madronich, S., and Aumont, B.: Impact of chamber wall loss of gaseous organic compounds on secondary organic aerosol formation: explicit modeling of SOA formation from alkane and alkene oxidation, *Atmos. Chem. Phys.*, 16, 1417-1431, 10.5194/acp-16-1417-2016, 2016.
- Leahy, D. E., Morris, J. J., Taylor, P. J., and Wait, A. R.: Model solvent systems for QSAR. Part 3. An LSER analysis of the 'critical quartet.' New light on hydrogen bond strength and directionality, *Journal of the Chemical Society, Perkin Transactions 2*, 705-722, 10.1039/p29920000705, 1992.
- 610 Li, J., Li, K., Li, H., Wang, X., Wang, W., Wang, K., and Ge, M.: Long-chain alkanes in the atmosphere: A review, *Journal of Environmental Sciences*, 114, 37-52, <https://doi.org/10.1016/j.jes.2021.07.021>, 2022.
- Lim, Y. B. and Ziemann, P. J.: Effects of Molecular Structure on Aerosol Yields from OH Radical-Initiated Reactions of Linear, Branched, and Cyclic Alkanes in the Presence of NO_x, *Environmental Science & Technology*, 43, 2328-2334, 10.1021/es803389s, 2009.
- 615 Madhu, A., Jang, M., and Deacon, D.: Modeling the influence of chain length on secondary organic aerosol (SOA) formation via multiphase reactions of alkanes, *Atmos. Chem. Phys.*, 23, 1661-1675, 10.5194/acp-23-1661-2023, 2023.
- Manavi, S. E. I. and Pandis, S. N.: A lumped species approach for the simulation of secondary organic aerosol production from intermediate-volatility organic compounds (IVOCs): application to road transport in PMCAMx-iv (v1.0), *Geosci. Model Dev.*, 15, 7731-7749, 10.5194/gmd-15-7731-2022, 2022.
- Massolo, L., Rehwagen, M., Porta, A., Ronco, A., Herbarth, O., and Mueller, A.: Indoor-outdoor distribution and risk assessment of volatile organic compounds in the atmosphere of industrial and urban areas, *Environmental Toxicology*, 25, 339-349, <https://doi.org/10.1002/tox.20504>, 2010.
- 625 McMurry, P. H. and Grosjean, D.: Gas and aerosol wall losses in Teflon film smog chambers, *Environmental science & technology*, 19, 1176-1182, 1985.
- Murphy, B. N., Sonntag, D., Seltzer, K. M., Pye, H. O. T., Allen, C., Murray, E., Toro, C., Gentner, D. R., Huang, C., Jathar, S. H., Li, L., May, A. A., and Robinson, A. L.: Reactive Organic Carbon Air Emissions from Mobile Sources in the United States, *EGUsphere*, 2023, 1-24, 10.5194/egusphere-2023-855, 2023.
- 630 Myrdal, P. B. and Yalkowsky, S. H.: Estimating Pure Component Vapor Pressures of Complex Organic Molecules, *Industrial & Engineering Chemistry Research*, 36, 2494-2499, 10.1021/ie950242l, 1997.
- Nel, A.: Air Pollution-Related Illness: Effects of Particles, *Science*, 308, 804-806, 10.1126/science.1108752, 2005.
- Odian, G.: Principles of polymerization, John Wiley & Sons 2004.
- 635 Platts, J. A., Butina, D., Abraham, M. H., and Hersey, A.: Estimation of Molecular Linear Free Energy Relation Descriptors Using a Group Contribution Approach, *Journal of Chemical Information and Computer Sciences*, 39, 835-845, 10.1021/ci980339t, 1999.
- Press, W. H., Flannery, B. P., Teukolsky, S. A., and Vetterling, W. T.: Newton-Raphson method using derivative and Newton-Raphson method for nonlinear systems of equations. *Numerical Recipes in FORTRAN: The Art of Scientific Computing*, 1992.
- 640 Puzyn, T., Leszczynski, J., and Cronin, M. T.: Recent advances in QSAR studies: methods and applications, 2010.
- Pye Havalala, O. T., D'Ambro Emma, L., Lee Ben, H., Schobesberger, S., Takeuchi, M., Zhao, Y., Lopez-Hilfiker, F., Liu, J., Shilling John, E., Xing, J., Mathur, R., Middlebrook Ann, M., Liao, J., Welti, A., Graus, M., Warneke, C., de Gouw Joost, A., Holloway John, S., Ryerson Thomas, B., Pollack Ilana, B., and Thornton Joel, A.: Anthropogenic enhancements to production of highly oxygenated molecules from autoxidation, *Proceedings of the National Academy of Sciences*, 116, 6641-6646, 10.1073/pnas.1810774116, 2019.
- 645



- Reid, J. P., Bertram, A. K., Topping, D. O., Laskin, A., Martin, S. T., Petters, M. D., Pope, F. D., and Rovelli, G.: The viscosity of atmospherically relevant organic particles, *Nature Communications*, 9, 956, 10.1038/s41467-018-03027-z, 2018.
- Roldin, P., Ehn, M., Kurtén, T., Olenius, T., Rissanen, M. P., Sarnela, N., Elm, J., Rantala, P., Hao, L., Hyttinen, N., Heikkinen, L., Worsnop, D. R., Pichelstorfer, L., Xavier, C., Clusius, P., Öström, E., Petäjä, T., Kulmala, M., Vehkamäki, H., Virtanen, A., Riipinen, I., and Boy, M.: The role of highly oxygenated organic molecules in the Boreal aerosol-cloud-climate system, *Nature Communications*, 10, 4370, 10.1038/s41467-019-12338-8, 2019.
- 650 Sazhin, S. S., Al Qubeissi, M., Nasiri, R., Gun'ko, V. M., Elwardany, A. E., Lemoine, F., Grisch, F., and Heikal, M. R.: A multi-dimensional quasi-discrete model for the analysis of Diesel fuel droplet heating and evaporation, *Fuel*, 129, 238-266, <https://doi.org/10.1016/j.fuel.2014.03.028>, 2014.
- 655 Schell, B., Ackermann, I. J., Hass, H., Binkowski, F. S., and Ebel, A.: Modeling the formation of secondary organic aerosol within a comprehensive air quality model system, *Journal of Geophysical Research: Atmospheres*, 106, 28275-28293, <https://doi.org/10.1029/2001JD000384>, 2001.
- Shrivastava, M., Cappa, C. D., Fan, J., Goldstein, A. H., Guenther, A. B., Jimenez, J. L., Kuang, C., Laskin, A., Martin, S. T., Ng, N. L., Petaja, T., Pierce, J. R., Rasch, P. J., Roldin, P., Seinfeld, J. H., Shilling, J., Smith, J. N., Thornton, J. A., Volkamer, R., Wang, J., Worsnop, D. R., Zaveri, R. A., Zelenyuk, A., and Zhang, Q.: Recent advances in understanding secondary organic aerosol: Implications for global climate forcing, *Reviews of Geophysics*, 55, 509-559, <https://doi.org/10.1002/2016RG000540>, 2017.
- 660 Song, C., Liu, B., Dai, Q., Li, H., and Mao, H.: Temperature dependence and source apportionment of volatile organic compounds (VOCs) at an urban site on the north China plain, *Atmospheric Environment*, 207, 167-181, <https://doi.org/10.1016/j.atmosenv.2019.03.030>, 2019.
- 665 Tkacik, D. S., Presto, A. A., Donahue, N. M., and Robinson, A. L.: Secondary Organic Aerosol Formation from Intermediate-Volatility Organic Compounds: Cyclic, Linear, and Branched Alkanes, *Environmental Science & Technology*, 46, 8773-8781, 10.1021/es301112c, 2012.
- World Health, O.: Ambient air pollution: a global assessment of exposure and burden of disease, World Health Organization, Geneva2016.
- 670 Wu, L., Wang, X., Lu, S., Shao, M., and Ling, Z.: Emission inventory of semi-volatile and intermediate-volatility organic compounds and their effects on secondary organic aerosol over the Pearl River Delta region, *Atmos. Chem. Phys.*, 19, 8141-8161, 10.5194/acp-19-8141-2019, 2019.
- Xavier, C., Rusanen, A., Zhou, P., Dean, C., Pichelstorfer, L., Roldin, P., and Boy, M.: Aerosol mass yields of selected biogenic volatile organic compounds – a theoretical study with nearly explicit gas-phase chemistry, *Atmos. Chem. Phys.*, 19, 13741-13758, 10.5194/acp-19-13741-2019, 2019.
- 675 Xuan, L., Ma, Y., Xing, Y., Meng, Q., Song, J., Chen, T., Wang, H., Wang, P., Zhang, Y., and Gao, P.: Source, temporal variation and health risk of volatile organic compounds (VOCs) from urban traffic in harbin, China, *Environmental Pollution*, 270, 116074, <https://doi.org/10.1016/j.envpol.2020.116074>, 2021.
- 680 Yang, W., Li, J., Wang, W., Li, J., Ge, M., Sun, Y., Chen, X., Ge, B., Tong, S., Wang, Q., and Wang, Z.: Investigating secondary organic aerosol formation pathways in China during 2014, *Atmospheric Environment*, 213, 133-147, <https://doi.org/10.1016/j.atmosenv.2019.05.057>, 2019.
- Yap, C. W.: PaDEL-descriptor: An open source software to calculate molecular descriptors and fingerprints, *Journal of Computational Chemistry*, 32, 1466-1474, <https://doi.org/10.1002/jcc.21707>, 2011.
- 685 Yu, Z., Jang, M., and Madhu, A.: Prediction of Phase State of Secondary Organic Aerosol Internally Mixed with Aqueous Inorganic Salts, *The Journal of Physical Chemistry A*, 125, 10198-10206, 10.1021/acs.jpca.1c06773, 2021a.
- Yu, Z., Jang, M., Zhang, T., Madhu, A., and Han, S.: Simulation of Monoterpene SOA Formation by Multiphase Reactions Using Explicit Mechanisms, *ACS Earth and Space Chemistry*, 5, 1455-1467, 10.1021/acsearthspacechem.1c00056, 2021b.
- 690 Zhao, L., Li, P., and Yalkowsky, S. H.: Predicting the Entropy of Boiling for Organic Compounds, *Journal of Chemical Information and Computer Sciences*, 39, 1112-1116, 10.1021/ci990054w, 1999.
- Zhao, Q., Bi, J., Liu, Q., Ling, Z., Shen, G., Chen, F., Qiao, Y., Li, C., and Ma, Z.: Sources of volatile organic compounds and policy implications for regional ozone pollution control in an urban location of Nanjing, East China, *Atmos. Chem. Phys.*, 20, 3905-3919, 10.5194/acp-20-3905-2020, 2020.



695 Zhou, C., Jang, M., and Yu, Z.: Simulation of SOA formation from the photooxidation of monoalkylbenzenes in the presence
of aqueous aerosols containing electrolytes under various NO_x levels, *Atmos. Chem. Phys.*, 19, 5719-5735, 10.5194/acp-19-
5719-2019, 2019.

700 Zuend, A., Marcolli, C., Booth, A. M., Lienhard, D. M., Soonsin, V., Krieger, U. K., Topping, D. O., McFiggans, G., Peter,
T., and Seinfeld, J. H.: New and extended parameterization of the thermodynamic model AIOMFAC: calculation of activity
coefficients for organic-inorganic mixtures containing carboxyl, hydroxyl, carbonyl, ether, ester, alkenyl, alkyl, and aromatic
functional groups, *Atmos. Chem. Phys.*, 11, 9155-9206, 10.5194/acp-11-9155-2011, 2011.